Application of Stability Analysis of $Q(V)$-Characteristic Controls Related to the Converter-Driven Stability in Distribution Networks

Sebastian Krahmer, Stefan Ecklebe, Peter Schegner, *Senior Member, IEEE*, and Klaus Röbenack

***Abstract*—As the amount of volatile, renewable energy sources in power distribution networks is increasing, the stability analysis of the latter is a vital aspect for network operators. Within the STABEEL project, the authors develop rules on how to parameterize the reactive power control of distributed energy resources to increase the performance while guaranteeing voltage stability. The work focuses on distribution networks with a high penetration of distributed energy resources equipped with $Q(V)$-characteristics. This contribution is based on the stability assessment of previous work and introduces a new approach using the Circle Criterion. Herein, distributed energy resources can be modeled as detailed control loops or as approximations, derived from technical guidelines. In addition, the wavelet transform is applied to RMS time series simulations to obtain a more realistic, less conservative reference. With the aim of extending existing technical guidelines, the stability assessment methods are applied to distribution networks.**

***Index Terms*—Converter-driven stability, droop control, Q(V), stability criteria, voltage control, voltage stability, volt/var.**

I. Introduction

ACROSS Europe, a massive growth of distributed energy resources (DERs) based on wind and solar energy can be observed. These changes require not only an adaption of the existing electrical power networks but also of their operation in terms of voltage control or reactive power provisioning. The network operators can meet these challenges by employing a combination of centralized and distributed voltage control concepts. One method of indirect voltage control is the $Q(V)$-control, which implements an adaption of the system reactive power depending on the voltage level at the network connection point with a $Q(V)$-characteristic [1]. Previous contributions show possible applications with regard to *i*) cost-effectiveness and efficiency [2], [3], [4], *ii*) optimal (local) voltage management [3], [5], [6], [7], [8], [9], *iii*) fallback voltage support [10] or *iv*) optimal power flow [11], [12] in distribution networks (DNs). However, all operational strategies must meet stability requirements.

Possible interactions of $Q(V)$-characteristic controls are classified as (short-time) voltage stability or as *slow-interaction converter-driven stability*, newly introduced in [13]. Considering $Q(V)$-characteristic control, network codes, such as RfG [14], are very restrictive regarding parameterization limits, which counteract a more network-serving application. However, especially in weak networks the distribution network operators (DSOs) must be aware of voltage control interactions, as shown in [15], [16]. These interactions must continue to be investigated and an extended generic computation approach should be provided to DSOs. The STABEEL[1] project addresses the development of rules for assessing the stability of DER controls in electrical power systems.

A. Relevant Literature

In response to the aforementioned challenges, several contributions on related stability aspects have been published, especially to low-voltage (LV) DNs. Aspects considered include instability at large controller dead times [17] and the influence of damping time constants [4], [18]. The authors of [19] analyze small-signal stability using the Nyquist criterion, focusing on single-input single-output systems. They conclude that all dynamics in the same time domain must be considered for parameterization, while [20] explicitly states that faster voltage measurement and averaging leads to reduced stability margins.

With respect to multiple-input-multiple-output (MIMO) systems, [18] states that for DER-dominated low-voltage grids, there are no (practically relevant) restrictions on the use of $Q(V)$ characteristic-based control for photovoltaics (PV) if basic parameterization rules are followed. Furthermore, the contributions [5], [7], [9], [21] show procedures for the optimization of local $Q(V)$-controls regarding individual needs based on stability analysis in the time-discrete domain. Here,

Manuscript received 28 August 2023; revised 1 December 2023; accepted 10 January 2024. Date of publication 30 January 2024; date of current version 21 May 2024. Paper 2023-IACC-1094.R1, presented at the 2022 International Conference on Smart Energy Systems and Technologies, Eindhoven, The Netherlands, Sep. 05–07, and approved for publication in the IEEE Transactions on Industry Applications by the Industrial Automation and Control Committee of the IEEE Industry Applications Society [DOI: 10.1109/SEST53650.2022.9898506]. This work was supported in part by the joint publication funds of the TU Dresden, the SLUB Dresden and the Open Access Publication Funding of the DFG. This research was founded by the Deutsche Forschungsgemeinschaft (DFG, DOI: 10.13039/501100001659) – project no. 442893506. *(Corresponding author: Sebastian Krahmer.)*

Sebastian Krahmer and Peter Schegner are with the Chair of Electrical Energy Supply, TUD Dresden University of Technology, 01062 Dresden, Germany (e-mail: sebastian.krahmer@tu-dresden.de; peter.schegner@tu-dresden.de).

Stefan Ecklebe and Klaus Röbenack are with the Instiute of Control Theory, TUD Dresden University of Technology, 01062 Dresden, Germany (e-mail: stefan.ecklebe@tu-dresden.de; klaus.roebenack@tu-dresden.de).

Color versions of one or more figures in this article are available at https://doi.org/10.1109/TIA.2024.3360023.

Digital Object Identifier 10.1109/TIA.2024.3360023

[1] A brief project description can be found at https://tud.link/2me9.

so-termed non-incremental $Q(V)$-rules without delay components have been studied by the latter two, which are jointly based on [22]. Incorporating the dynamic of the DER control transfer function, [5] and [7] rely on the stability analysis of [23]. In addition, [24] discusses trade offs between the local gains of $Q(V)$-controlled DERs and the rate of convergence of the system after a fault using the network model of [22] and arrive at a similar stability analysis formulation as [23]. Finally, [25] extends the work of [24] by introducing an operating point dependent network model (i.e. nodal voltage sensitivities).

At higher voltage levels, single DERs are grouped together and then equipped with farm control. Furthermore, a communication delay within farm control must be taken into account at this point [26]. However, the case of DERs directly connected to the medium (MV) and high voltage (HV) network with $Q(V)$-characteristic control, which differs from the above cases in terms of network topology and installed plant capacity, has been less studied so far. Due to this, a stability assessment for MV and HV levels with focus on wind farm (WF) models was introduced in previous work [27] using a time-continuous model. This approach incorporates the maximum transfer function gain of each single DER, but results in conservative thresholds, i.e. remains in parts below the network code recommendations. The elaborated stability assessment approach shows strong parallels to [24], [25]. In addition, in [28] the authors showed that the problem of nonlinear operating point-dependent network feedback can be represented by a second-order network model approximation. Alternatively, with detailed knowledge of the system, a root mean squared (RMS) simulation and evaluation is possible by using network computation software such as *DIgSILENT PowerFactory*. Regarding the automatic analysis of the simulated time series, the state of the art includes time-domain approaches (e.g. integral absolute error and auto correlation), frequency domain approaches (e.g. fast Fourier transform), as well as hybrid approaches (e.g. wavelet transform) next to methods based on artificial neural networks (cf. [29], [30]). Furthermore, various practical applications of the wavelet transform show promising results [31], [32].

B. Contributions and Organization

The objective of this work is the stability assessment (SA) of interconnected $Q(V)$-controlled DERs modeled in the time-continuous domain. The contributions are based on [1] and cover three fronts: *i*) Modeling of the feedback systems used by different DER types in distribution grids. In the absence of information on detailed DER models, the derivation of a second order linear transfer function as representative approximation is shown. *ii*) Derivation of an analytic criterion for the SA of interacting $Q(V)$-controlled DERs or voltage controllers in MV and HV networks. This novel approach is based on the so-called Circle Criterion. By incorporating the interaction dynamics of the control, this approach is characterized by a lower degree of conservatism compared to previous work [27]. We point out that more accurate information about DER models results in better outcomes of the SA. *iii*) By introducing practical evaluation thresholds, the wavelet transform is applied to time series of RMS quantities for automatic SA. This approach can be used for near real-time SA based on measurement time series or for verification of analytical methods based on RMS simulations in network computation software. The evaluation process is depicted in Fig. 1. The comprehensive software implementation of this case study is available as a *Code Ocean capsule* [33].

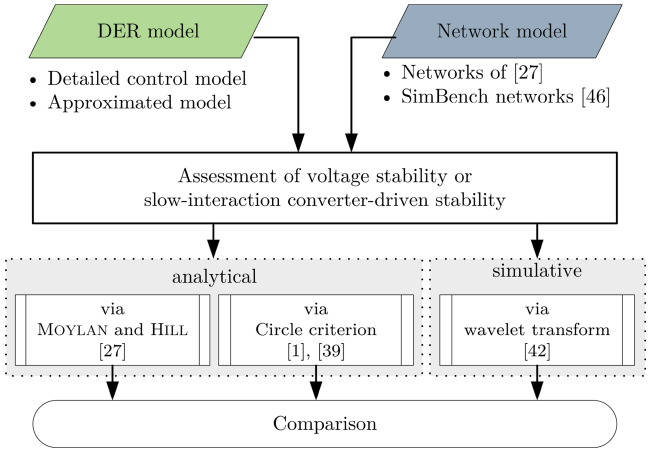

Fig. 1. Overview of the analytical and simulative stability assessment methods used in this paper and the input data required.

The proposed work is organized as follows: Section II explores the power system modeling including DERs with $Q(V)$-characteristic. In Section III, the authors propose various DER models, which can be expressed by detailed control loops or by approximated models. Then, the SA of nonlinear systems utilizing the Circle Criterion is introduced in Section IV. In the next section, a posteriori SA of simulated or measured time series using the wavelet transform is presented and the application to voltage histories is discussed. In VI, the presented SA methods are applied to various HV benchmark networks. The results are compared with the findings of previous work [27] and RMS time domain simulations of detailed modeled systems. Finally, conclusions are drawn in Section VII.

Notation: Column vectors (matrices) are denoted by bold lower-(upper-) case letters and $\boldsymbol{I}$ is the identity matrix. Complex values are underlined and * takes the complex conjugate.

II. System Model

This section provides a brief summary of the voltage control loop of $Q(V)$-controlled DERs. The complete control loop consists of the $Q(V)$-characteristic, which calculates a desired reactive power from the nodal voltage, which then, shaped by a plant-specific control loop, finally feeds a static linear network model, which in turn results in the new nodal voltage. Fig. 2 shows this overall system model for the MIMO case assuming a DN with n $Q(V)$-controlled nodes. The components of the system are explained in more detail below.

A. Q(V)-Characteristic Curve

The $Q(V)$-characteristic is a nonlinear function that maps the measured nodal voltage at the point of common coupling U_{PCC}

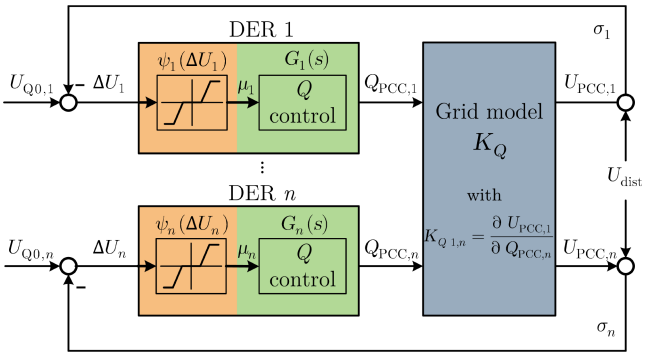

Fig. 2. Generic reactive power control path for MIMO case, adapted to a $Q(V)$-characteristic control.

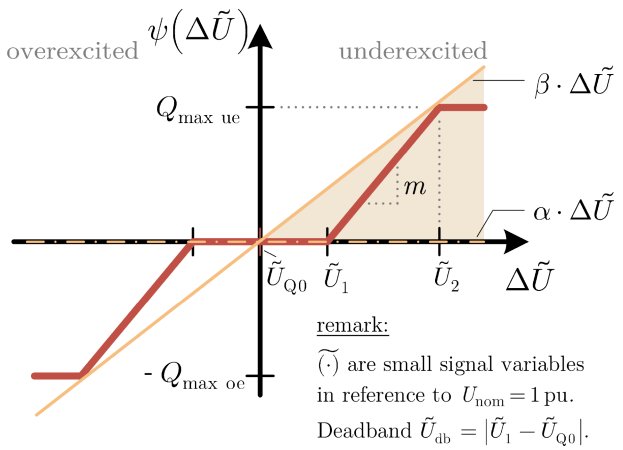

Fig. 3. $Q(V)$-characteristic $\psi(\Delta U)$ with an enclosing sector area.

to a desired reactive power and is shown in Fig. 3. It exhibits areas of saturation as well as a deadband, between which it is monotonically increasing. As introduced in previous work [27] and depicted in Fig. 3, the nonlinear $Q(V)$-characteristic can be generally represented by a sector enclosing this $Q(V)$-curve $\psi(\Delta U)$ between two linear functions with slope α and β, respectively. Here, ΔU is the deviation of the measured voltage from the origin of the characteristic U_{Q0}, which is not necessarily the nominal voltage U_{nom}[2]. Using this approach, even characteristics with variable or optimized "curved" slopes m as well as asymmetric slopes can be taken into account. For the cases considered in this publication, by denoting the rated active power with P_r the linear slope m is given as:

$$m := \frac{\Delta Q/P_r}{\Delta U/U_{nom}} \text{ with } [m] = \frac{\%}{\text{pu}}. \tag{1}$$

In the following, $\psi(\Delta U)$ is bounded by the x-axis from below and by a linear function with slope $\beta > 0$ from above.

[2]To accurately represent this relation, all voltage variables in Fig. 3 are related to the nominal voltage and represented by $\widetilde{(\cdot)}$.

B. Static Network Model

Within this contribution, all DERs are assumed to be coupled through a common static network, modeled by the constant nodal voltage sensitivity matrix $\boldsymbol{K}_Q \in \mathbb{R}^{n\times n}$ [27]. For the computation of this simplified network model, one starts with the apparent power equations of the network and does some transformations. The complex apparent power in each network node can be calculated from the complex vector of line-to-ground nodal voltages $\underline{\boldsymbol{u}}$ via

$$\underline{\boldsymbol{s}} = 3\ \text{diag}\,(\underline{\boldsymbol{u}})\,\underline{\boldsymbol{Y}}^*\underline{\boldsymbol{u}}^* = \boldsymbol{p} + \text{j}\boldsymbol{q}, \tag{2}$$

wherein $\underline{\boldsymbol{Y}}$ represents the node admittance matrix of the network.

For a given power system operating point, the JACOBIAN of the apparent power related to the complex voltage $\boldsymbol{J} \in \mathbb{R}^{2n\times 2n}$ can be obtained by linearization[3] using the node admittance matrix of the network $\underline{\boldsymbol{Y}}$ (2), cf. [34, Eq. 5.114]. The operating point $\mathcal{O}$ is defined by complex nodal voltages corresponding to the distribution of active and reactive load power. Then, the nodal voltage sensitivity matrix $\boldsymbol{K}_Q$ can be obtained by inversion of $\boldsymbol{J}$ and subsequent selection of the submatrix with respect to the ith element definition $K_{Q\,i,i} = \frac{\partial U_i}{\partial Q_i}$, $i = 1, \ldots, n$, cf. Fig. 2. We would like to point out that the influence of the reactive power on the voltage magnitude is only dominant if $X/R \gg 1$ holds for the networks impedance-resistance ratio. Therefore, especially in low voltage networks the voltage disturbance U_{dist} in Fig. 2 may have a bigger influence on the change in voltage.

C. Multi-Input Multi-Output System Model

The underlying technology and operating mode of each DER have an impact on the reactive control path representation. However, assuming a normal operation mode and neglecting reactive power constraints at low active power infeed, the reactive power control path can be treated separately from the remaining plant model. As many different models can be used here, Section III will give a detailed overview of relevant plant models that are related to the DER technology or to a PT_2 representation, respectively. As depicted in Fig. 2, the reactive power control loop $G_i(s)$, $i = 1, \ldots, n$ of each plant can be separated from the nonlinear $Q(V)$-characteristic $\psi_i(\Delta U_i)$, $i = 1, \ldots, n$ regardless of the fashion in which the control is implemented inside of $G_i(s)$.

Subsequently, writing $\boldsymbol{\mu}(s) := (\mu_1(s), \ldots, \mu_n(s))^\top \in \mathbb{R}^n$ for the input and $\boldsymbol{\sigma}(s) := (\sigma_1(s), \ldots, \sigma_n(s))^\top \in \mathbb{R}^n$ for the output vector as well as pooling the independent transfer functions in $\boldsymbol{G}(s) := \text{diag}(G_1(s), \ldots, G_n(s))$, the system dynamics can be written as

$$\boldsymbol{\sigma}(s) = \tilde{\boldsymbol{G}}(s)\boldsymbol{\mu}(s) \tag{3a}$$

$$\boldsymbol{\mu}(s) = \boldsymbol{\psi}(\boldsymbol{\sigma}(s)) \tag{3b}$$

(cf. Fig. 2 with $U_{Q0,i} = U_{dist} = 0$) with the overall transfer function matrix $\tilde{\boldsymbol{G}}(s) := \boldsymbol{G}(s)\boldsymbol{K}_Q$.

As this contribution assumes balanced single-line network models, the presented approach would need to be extended for

[3]For a more detailed consideration, see [25].

TABLE I
OVERVIEW OF THE APPLICATION OF THE SA CRITERIA RELATED TO THE KNOWLEDGE OF DER MODELS

SA class	Knowledge of DER plant model		
	None	Blackbox	Whitebox
Analytical	Robust with PT_2-TAR	Robust with PT_2-DER	Robust
	Circle with PT_2-TAR	Circle with PT_2-DER	Circle
Simulative	-	Wavelet	Wavelet

unbalanced networks. Additionally, a more realistic, i.e. voltage dependent network model is presented in [28] by including the derivative of $\boldsymbol{K}_Q(\boldsymbol{\Delta u})$, but is not used in this contribution, since it adds an additional nonlinearity. In this respect, an alternative time-discrete modeling approach is discussed in [25].

III. PLANT MODELS

In this section, we summarize different DER models $G(s)$ from the literature and integrate them into the system model of (3). Furthermore, for cases where neither the model parameters nor the detailed model structure are known, two alternative approaches are presented, referred to as PT_2-DER and PT_2-TAR. The first approach assumes that the DER operator does not supply a detailed model to the stability assessor, but provides a model approximation, e.g. in form of a PT_2-element. The second approach can be interpreted as a fallback, for the case that a detailed model or even an approximation based on this model is not available. Finally, a comparison is drawn on the example of a wind farm.

A. Detailed Models of Voltage Control in Distributed Energy Resources (Orig. DER)

Normative publications and research work such as [35], [36], [37], [38] provide complex models of almost all different DER types. Furthermore, regarding the Q-control dynamics $G_i(s)$ the authors focus on three popular DER types: (i) WF of type fully rated converter (FRC), (ii) WF of type double fed induction generator (DFIG), (iii) photovoltaic farm (PVF), whose detailed models and parameterizations are given in Table II. Note that other inverter-driven energy resources, such as FACTS or battery storage, are not explicitly considered here due to their highly adaptable inverter behavior.

All mentioned DER models can be extended by adding a farm control unit containing logic of the $Q(V)$-characteristic as well as additional measurements and delay blocks. The migration from individual unit control to farm control is characterized by an additional communication delay. This dead time block with the time constant T_g is set between the setpoint tracking Q_R and unit/inverter current control $\tilde{Q}_{set}$. Furthermore, a voltage-averaging block feeds into the $Q(V)$-characteristic, which further feeds into the reactive power control loop of the DER. However, as voltage-averaging has a gain of 1, the $Q(V)$-characteristic $\psi(\Delta U)$ can be swapped with it and combined with the downstream reactive power control loop [27]. Thus, one arrives at the summarized reactive power control loop $G(s)$ shown in Table II.

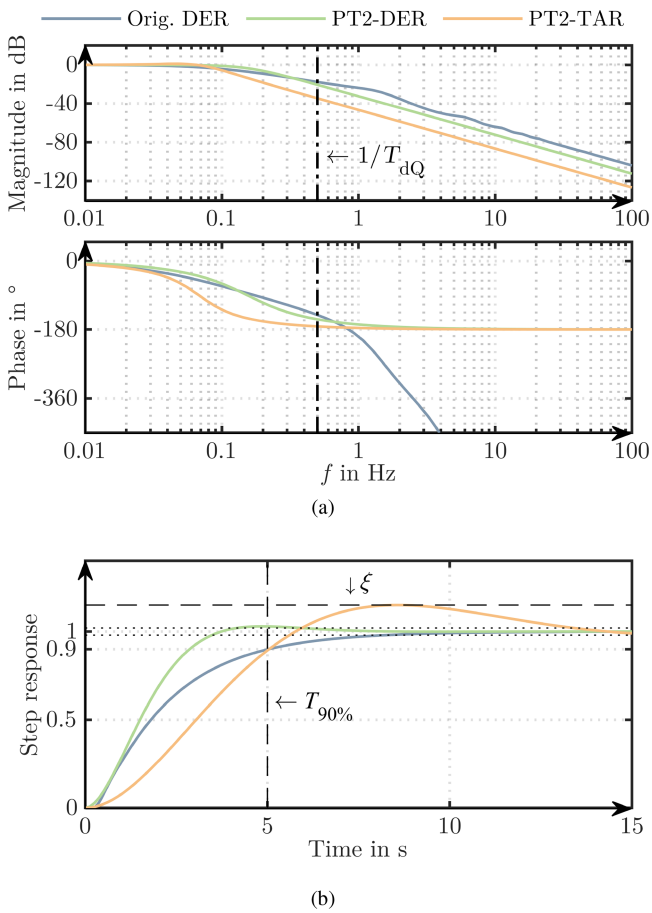

Fig. 4. Comparison of frequency and step responses of a detailed DER model (Orig. DER) with PT_2-approximations based on detailed DER model and generic TAR step response, respectively. A WF-FRC is used as DER model and the model parameterizations can be obtained from Table II. (a) Frequency response with kink frequency of the dominant DER PT1 element. (b) Step response with characteristic overshoot and rise time quantities.

B. PT_2-Fit Based on the Frequency Response of a Specific DER Model (PT_2-DER)

Using the detailed DER model as fitting target, a realistic approximation can be provided by fitting a second order linear transfer function (PT_2-element) to the frequency response of a fully parameterized, detailed DER model. The PT_2-element under consideration is of the form

$$G_{PT_2}(s) = \frac{1}{1 + 2DTs + T^2 s^2}, \tag{4}$$

where D is the damping factor and T is the characteristic frequency of the element. The drawback is the required specification of DER model parameters, which, however, are usually provided to the DSO when the DER is commissioned. For this approach, we are using the frequency response with respect to magnitude and angle within a relevant frequency band for PT_2 fitting, as shown in Fig. 4(a). This frequency band is derived from the bandwidth of the control loop inputs, as higher frequencies

TABLE II
PROPOSED MODEL CONFIGURATION OF DIFFERENT DER TYPES AND RELATED PT_2 APPROXIMATIONS

DER type	Control loop $G(s)$		Ref.
	Voltage averaging	Reactive power control loop	
(i) WF-FRC	$\frac{1}{1+sT_U}$, $T_U = 0.02\,s$	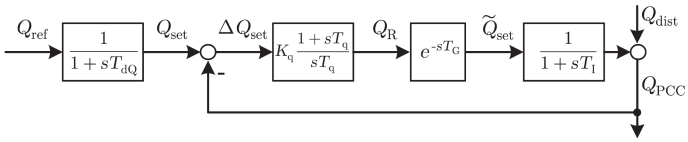 $T_{dQ} = 2\,s$, $K_q = 0.5$, $T_q = 0.2\,s$, $T_I = 0.1\,s$, $T_g = 0.2\,s$	[27], [37]
(ii) WF-DFIG		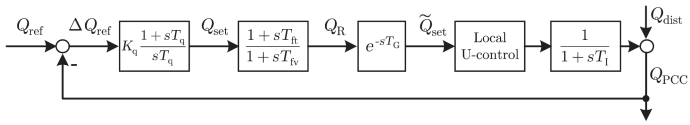	[27], [35]
(iii) PVF	$\frac{1}{(1+sT_U)^3}$, $T_U \approx 0.004\,s$	A PV inverter with fast power control settings (cf. T_I in [38]) extended by a farm control. The emerging control loop can be established analogously to (i) with $T_{dQ} = 2\,s$, $K_q = 0.5$, $T_q = 0.2\,s$, $T_I = 0.0033\,s$, $T_g = 0.2\,s$.	[38]
(iv) PT_2-TAR	Not necessary	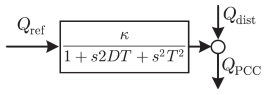 Based on the generic step response given in TAR with $\kappa = 1$, $D = 0.517$, $T = 2.335\,s$.	[39]
(v) PT_2-DER		Based on the frequency response of detailed DER model (i) with $\kappa = 1$, $D = 0.747$, $T = 1.028\,s$.	

are filtered out in the previous layers. The lower bound can be defined by the transformer tap control and the upper bound can be set at twice the voltage averaging time constant. Therefore, for the PT_2 fit it follows that frequency f is in the interval from 0.01 Hz to 100 Hz. Furthermore, the PT_2 static gain is fixed to 1 to match the static gain of the detailed model, cf. Fig. 4(b). Table II shows the obtained PT_2 parameters.

C. PT_2-Fit Based on Technical Guidelines (PT_2-TAR)

When connecting DERs to DNs, technical guidelines apply, which regulate, e.g., the way in which reactive power is provided [14]. Thus, specifications on the principle dynamics of reactive power provision are defined. The incorporation of these boundaries for a control response allows a reduction of model complexity toward a PT_2 representation.

The German technical guideline [39] (TAR) provides such a specification for the set of admissible control behaviors, by means of parameterization of a generic step response. The TAR specifies the three characteristic parameters maximum overshoot ξ, rise time to first reach 90 % of static gain $T_{90\%}$ as well as settling time T_{stl} to reach a tolerance band around the static gain. Assuming a "slow" parameterized DER, ξ is set to 15 %, $T_{90\%} = 5\,s$ and T_{stl} should around $T_{90\%} + 3\,s$. An optimization algorithm based on least squares was used to fit a PT_2-element of (4). Thereby, the overshoot ξ, the rise time $T_{90\%}$ and the settling time T_{stl} are to be reproduced with only two degrees of freedom D, T, assuming that the static gain was set to 1 to match the static gain of the step response. As shown in Fig. 4(b), a match of ξ and $T_{90\%}$ were weighted more significantly, because of the high impact on dynamic system response. Table II shows the obtained PT_2 parameters.

D. Comparison of Detailed and Approximated DER Models

Fig. 4 shows the comparison of frequency and step responses of a detailed DER model with its PT_2 approximations. A WF-FRC model was used in this case, cf. Table II (i).

The evaluation of the frequency response in Fig. 4(a) shows that PT_2-DER hits the magnitude in a sufficient manner, but underestimates for higher frequencies. As a mitigation for this deficit, it can be considered that the largest time constant in the DER control loop T_{dQ} significantly attenuates higher frequencies. In conclusion, adaptable PT_2 approximations can be used to safely emulate the original DER behavior in the relevant frequency range (left side of $1/T_{dQ}$ in Fig. 4(a)).

Fig. 4(b) depicts the step responses, allowing the differences in the approximation to be determined. While the approximation based on TAR hits $T_{90\%}$ accurately, the overshoot ξ is assumed to be worse compared to the real DER model. In contrast, the approximation based on detailed DER has less $T_{90\%}$ and only slight overshoot ξ. This is to be expected since the approximation was performed in the frequency domain but is acceptable since the static gain is still achieved accurately and quickly. Thus, the estimation is conservative as it includes a more critical behavior.

IV. STABILITY ASSESSMENT

Preliminary work [27] has introduced the stability criterion from MOYLAN & HILL to perform a stability assessment for systems with $Q(V)$-characteristic control. By using the *small gain theorem*, the maximum gain of the transfer function is used. This inevitably leads to conservative results. Assuming that the parameters of a DER control $G(s)$ are known, other stability methods can be used to also incorporate the dynamic control interactions. Under the condition of a deterministic applicability,

the so-called Circle Criterion [40] is revisited in this section and its application to the system model (3) is discussed.

A. Stability Criterion for DER MIMO System With Q(V)-Characteristics

First, we introduce the concept of sector nonlinearities:

Definition 1 (Sector Nonlinearity, cf. [40, Def. 6.2]): A (vector-valued) function $\boldsymbol{f}: \mathbb{R}^n \to \mathbb{R}^n$ is said to belong to the sector $[\boldsymbol{0}, \boldsymbol{K}]$ for a symmetric positive definite matrix $\boldsymbol{K} \in \mathbb{R}^{n\times n}$ if $\boldsymbol{f}(\boldsymbol{x})^\top(\boldsymbol{f}(\boldsymbol{x}) - \boldsymbol{K}\boldsymbol{x}) \leq 0$.

Thus, if a function $\boldsymbol{f}(\boldsymbol{x})$ fulfills Definition 1 for a certain $\boldsymbol{K}$, we write $\boldsymbol{f}(\boldsymbol{x}) \in [\boldsymbol{0}, \boldsymbol{K}]$. Taking further into account the nature of the nonlinear $Q(V)$-characteristics $\psi_i(\Delta U_i)$ – as shown in Fig. 3 – we are able to formulate the following variant of the Circle Criterion:

Theorem 1 (Stability of a MIMO DER system with $Q(V)$-characteristics): The system (3) with the slope matrix $\boldsymbol{M} := \mathrm{diag}(\beta_1, \ldots, \beta_n)$ is absolutely stable if $\boldsymbol{I} + \boldsymbol{M}\tilde{\boldsymbol{G}}(s)$ is strictly positive real.

Proof: As every DER possesses its own local $Q(V)$-control, the static nonlinearity $\boldsymbol{\psi}(\boldsymbol{\Delta u})$ is decoupled, i.e. $\mu_i = \psi_i(-\sigma_i)$ holds for $i = 1, \ldots, n$. Thus, $\psi_i(\Delta U_i) \in [0, \beta_i]$ by Definition 1 and consequently $\boldsymbol{\psi}(\boldsymbol{\Delta u}) \in [\boldsymbol{0}, \boldsymbol{K}]$ with $\boldsymbol{K} = \mathrm{diag}(\beta_1, \ldots, \beta_n) = \boldsymbol{M}$ symmetric and positive definite. Furthermore, due to the pointwise symmetry of $\psi_i(\Delta U_i)$ we have $\boldsymbol{\mu} = \boldsymbol{\psi}(-\boldsymbol{\sigma}) = -\boldsymbol{\psi}(\boldsymbol{\sigma})$ for the input in (3b). Finally, if $\boldsymbol{I} + \boldsymbol{M}\tilde{\boldsymbol{G}}(s)$ is strictly positive real, we obtain stability by means of the Circle Criterion [40, Th. 7.1]. ∎

Hence, given the slopes $\beta_1, \ldots, \beta_n$ of all characteristics Theorem 1 allows for a straight-forward SA of a network since the strict positive realness condition (SPRC) can be easily verified by the criterion presented in [41].

B. Application of the Criterion

Theorem 1 only verifies the stability of a network for a given set of slopes $\beta_i,\ i = 1, \ldots, n$. In practice however, one is often interested in the actual maximal values for the slopes for which closed-loop stability can still be guaranteed. Within this contribution, two cases are considered for this problem:

a) *Uniform slopes:* For this case, all DERs in the network are assumed to operate with the same parameter set, yielding a uniform parameter λ for all plants such that $\beta_i = \lambda$ for $i = 1, \ldots, n$.
b) *Uniform voltage support:* As the impact of reactive power provisioning differs for each DER due to variations in network topology and line parameters it can be beneficial to work with uniform settings for the actual voltage support ability. For each plant this metric is given by the product of the slope β_i with the local auto-sensitivity k_i, where $k_i,\ i = 1, \ldots, n$ is the i-th element from the main diagonal of the sensitivity matrix $\boldsymbol{K}_Q$. Hence, the actual plant slopes are given by $\beta_i = -\lambda/k_i$ for $i = 1, \ldots, n$.

For both cases, the task at hand can be written as an optimization problem in the surrogate variable λ, whose value is to be maximized while upholding the SPRC from Theorem 1. This yields the following general minimization problem

$$\begin{aligned} \min_{\lambda\in\mathbb{R}^+} \quad & \frac{1}{\lambda} \\ \text{s.t.} \quad & \boldsymbol{I} + \boldsymbol{M}\tilde{\boldsymbol{G}}(s) \text{ strictly positive real} \\ & \boldsymbol{M} = \begin{cases} \lambda \boldsymbol{I} & \text{case a)} \\ -\lambda\, \mathrm{diag}\,(1/k_1, \ldots, 1/k_n) & \text{case b)} \end{cases} \end{aligned} \tag{5}$$

which is to be solved.

V. Time Series Based Stability Assessment Using Wavelet Transform

In addition to analytical evaluation, the objective of this section is the comparative evaluation of time histories from either simulations or measurements. Here, the introduced DER models can be used for investigation of RMS simulations in network computation programs. The challenge consists in the automated determination of signal patterns and superimposed oscillations from signal sequences that may be affected by noise. Therefore, in the following, we revisit the wavelet transform as a technique for time-frequency analysis of waveforms. Based on this, the application is discussed using exemplary voltage time series.

A. The Concept of Wavelet Transform in Respect to Power System Applications

The wavelet transform is suitable for detection of multiple oscillations in non-stationary variables due to the capability in decomposing the variables to its components of different frequencies [31]. The distribution of these components is used for evaluation of the continuity as well as the relevance in respect to the basis magnitude. Here, an fully scalable modulated evaluation window is moved over the signal and a spectrum is computed for each position. Then, the scheme is repeated for a large number of scales to obtain a signal representation with multiple time-frequency resolutions. This provides both good time resolution for high-frequency signals and good frequency resolution for low-frequency signals.

Due to the successful use in time-frequency analysis [42], [43], we chose the continuous wavelet transform (CWT). The CWT can be written in the time domain as

$$\mathcal{W}_\Upsilon[f](s,\tau) := \frac{1}{\sqrt{|s|}} \int_{-\infty}^{\infty} \Upsilon\left(\frac{t-\tau}{s}\right) f(t)\,\mathrm{d}t, \tag{6}$$

where s is the scale factor, τ is the translation factor, $\Upsilon(t)$ is the mother wavelet to choose and $f(t)$ is the time series to transform. Here, the choice of the Morse wavelet[4] as the mother wavelet proves to be promising, as shown by the wide application in engineering disciplines [32] as well as the specific application in electrical re-balancing after network islanding [44] or after faults in hybrid AC/DC microgrids [45].

[4]In [32, Eq. (9)], the general Morse wavelet is expressed in the frequency domain. In this contribution, we rely on the default values for the parameter of symmetry $\gamma = 3$ and compactness $\beta = 20$.

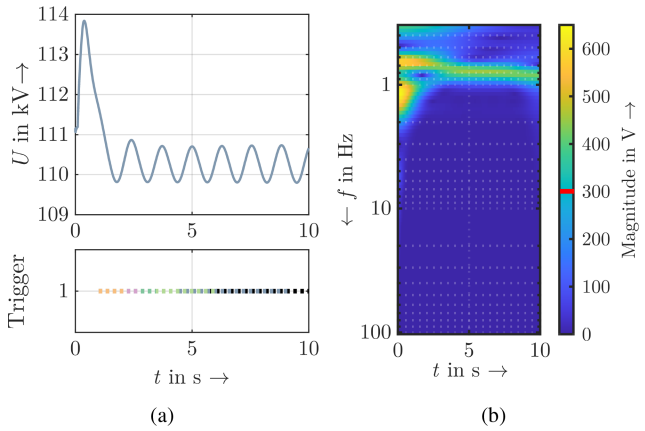

Fig. 5. Comparison of wave form and wavelet scalogram for nodal voltage on the example of a synthetic 110 kV network and a sampling rate of 1000 Hz. (a) RMS signal (upper) and threshold trigger for different frequency components (lower). (b) Wavelet scalogram with threshold δ (red line).

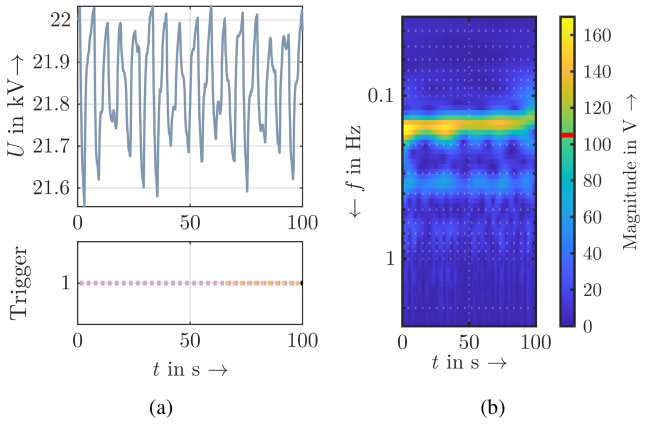

Fig. 6. Comparison of wave form and wavelet scalogram for nodal voltage on the example of a measured 21 kV network and a sampling rate of 5 Hz. (a) RMS signal (upper) and threshold trigger for different frequency components (lower). (b) Wavelet scalogram with threshold δ (red line).

B. Application of Wavelet Transform to RMS Time Series

By analyzing the RMS histories of relevant quantities such as nodal voltage or plant reactive power after a small-signal excitation or during long-term measurements, one can check retroactively for undesired behavior. Here, a suitable evaluation measure is the magnitude of detected frequency components. To do so, one can define a threshold above which the oscillation magnitude is classified as inadmissible in the form of

$$\delta = \min\{U_{\text{crit}}, u_{\text{crit}} \cdot U_{\text{nom}}\}, \tag{7}$$

where U_{crit} is a voltage level independent upper limit and u_{crit} is a factor relative to U_{nom}, which is the nominal line-to-line voltage of the node. Furthermore, for the delimitation of transient processes, a time span T_{crit} is specified, for which at least δ must be exceeded. The concrete threshold δ and the critical time span T_{crit} ought to be set by the DSO, e.g. based on the accuracy of the voltage measurement. In the following, two exemplary voltage time series depicted in Fig. 5 and Fig. 6 are discussed. In respect to (7), the threshold parameters are set to $U_{\text{crit}} = 300\,\text{V}$, $u_{\text{crit}} = 0.5\%$ and $T_{\text{crit}} = 2\,\text{s}$.

First, a synthetic 110 kV benchmark network was parameterized with a penetration rate of $Q(V)$-controlled DERs of 100 % and the DERs were parameterized with a $Q(V)$-characteristic slope $m = 60\ \%/\text{pu}$ to cause oscillations. The system was simulated for 10 s and as the event of excitation the $Q(V)$-control was activated at $t = 0\,\text{s}$. In Fig. 5(a) a voltage oscillation with a nearly constant frequency and magnitude is evident after the initial system response vanishes. The CWT result can be seen in Fig. 5(b) and shows how the magnitude of the signal's individual frequency components evolve over time. Herein, one can observe the parts of the frequency components that decay within the first two seconds as well as the lower frequency components that oscillate continuously from $t \approx 2\,\text{s}$ with a magnitude up to 450 V. As shown in the lower part of Fig. 5(a), a critical threshold violation was detected from the first time the critical evaluation time $T_{\text{crit}} = 2\,\text{s}$ was reached. The triggered critical frequency components of the RMS signal ranges from 0.59 Hz to 0.84 Hz. Note that the triggers for the different frequency components are not continuously active, but that at least one trigger is always present during the entire evaluation time.

Second, a 100 s long history was selected from a measurement of a WF captured at the 21 kV PCC. Fig. 6(a) shows superimposed voltage oscillations with variable magnitudes. The analysis of the CWT in Fig. 6(b) shows a continuous threshold violation for frequencies between 0.127 Hz to 0.18 Hz and period lengths of 5.5 s to 7.8 s, respectively. Note that the usability for measurement based time series is strongly influenced by the averaging interval of the RMS calculation. A longer averaging time may mask higher frequency oscillations.

With help of the wavelet transform time-critical threshold violations could be identified for individual frequencies in both example histories. To better distinguish between permissible and impermissible signal patterns, one can fine-tune the mother wavelet or adjust the evaluation time window for simulations in which the disturbance is known. The presented postponed assessment of voltage time series will be used in the next section for the automatic evaluation of power system simulations.

VI. Verification of Stability Assessment Criteria

The stability criterion, introduced in Section IV, is applied to four different HV networks. Thus, a comparison with the criterion introduced in [27] and stability bounds based on RMS simulations using the CWT based assessment from Section V is carried out.

A. Benchmark Networks

Four HV networks, two synthetic ones (sDN) and two realistic ones (rDN), are used for benchmarking purposes. All networks were parameterized with 100 % of the rated power of the consumer and generator loads. The sDN1 was introduced in [11], [27] and is characterized by a 100 % penetration rate of $Q(V)$-controlled nodes. The development of sDN2 was based

on realistic network data from Germany within the *SimBench* project [46]. Here, the variant *Mixed* has been modified by replacing the transformers of the network interconnection points with overhead line equivalents fed to a common 110 kV slack. Furthermore, all generators with a rated power greater than 1 MW were equipped with a $Q(V)$-control. Both rDNs are based on real topology data, but information on the control structures is missing. They are located in the area of the transmission system operator *50Hertz Transmission* in the eastern part of Germany and thereby represent lower DER penetration rates. It can be expected that the DER penetration rate will continue to increase clearly in the following decade. A detailed comparison of the penetration rate was done in [1, Tab. I].

B. Application Procedure

The aforementioned power networks have been implemented in *PowerFactory* and detailed frequency domain models of all DERs were created in the internal simulation language DSL. All DERs are of the WF-FRC type, cf. Table II, and equipped with a $Q(V)$-control. Further, it holds: *i*) each DER has the same slope m and *ii*) the $Q(V)$-characteristics contain no deadband, i.e. $\beta = m$[5]. Then, based on the given network topologies and using the three different DER plant model representations, the analytical SA is performed to obtain the maximum admissible slope β by means of (5), case (a). As a reference, RMS simulations were performed in *PowerFactory* and evaluated using the CWT. Table I provides a brief summary of the applicable methods.

The analytical SA predominantly relies on the topology and the operating point of the network. Therefore, an automatic export of the network data provided in *PowerFactory* to an interoperable JSON based power system data model [47] is executed using the open source toolbox *powerfactory-tools* [48]. Subsequently, the nodal voltage sensitivities $\boldsymbol{K}_Q$ are computed as required to build the linear transfer function matrix $\tilde{\boldsymbol{G}}(s)$ as in (3). Applying the presented Circle Criterion in (5) case (a), a critical slope β can be found.

For CWT based SA, the simulated nodal voltage responses were recorded for a duration of 15 s after a DER-external small signal disturbance occurs. Hereby, the cause of a disturbance can be a ramp or step in active power infeed of DERs, a step in the transformer ratio or voltage level respectively as well as a failure of a network asset. For simplification of evaluation, the active power feed-in of all DERs was increased ramp-like for the first 5 s. To be classified as stable, a nodal voltage oscillation must not violate the threshold $\delta = \min\{300\,\mathrm{V}, 0.05 \cdot U_{\mathrm{nom}}\}$ for a set duration $T_{\mathrm{crit}} = 1\,\mathrm{s}$ at the end of the evaluation window. It must therefore show significant decay within 10 s of the disturbance.

C. Discussion of Stability Assessment Results

Fig. 7 displays the comparison of the results for the SA introduced in Section IV (Circle) with the method presented in the previous study [27] (Robust) and reference evaluations based on simulated time series in *PowerFactory*, using the automatic CWT based SA (Wavelet). In addition, the Circle and Robust criterion were applied for the PT_2 plant models.

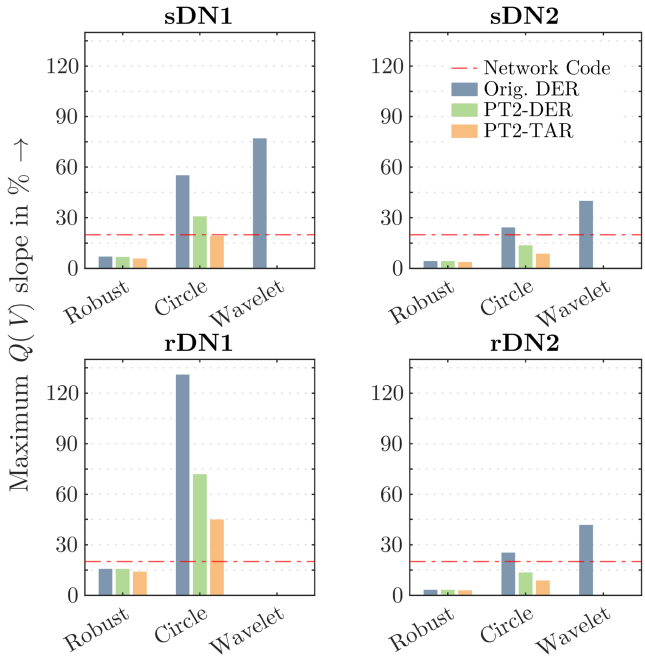

Fig. 7. Maximum admissible $Q(V)$ slopes as results of the SA (Robust, Circle, Wavelet). Three different DER models were implemented in each of the four HV benchmark networks. As reference the Orig. DER model is simulated in *PowerFactory* and evaluated using CWT. No limitation could be detected in rDN1 due to insufficient reactive power resources.

The maximum allowable slopes vary across the benchmark networks, as expected due to the differences in network structure and DER penetration. Specifically, using the DER model of type PT_2-TAR results in lower admissible slopes than with PT_2-DER, regardless of the stability criterion applied, due to a higher closed loop gain that is being assumed for the DER model[6]. This is not surprising since the PT_2-TAR model represents the worst DER behavior that is still allowed within the TAR specifications, where the PT_2-DER attempts to approximate the actual DER dynamics. Furthermore, it can be stated that the result using the Orig. DER model is the least conservative one. This effect is due to the conservative simplifications made. As conclusion for the control loop simplifications, the model PT_2-DER offers a shorter computing time in comparison to the Orig. DER due to the reduced model complexity and the model PT_2-TAR allows the application even without knowledge of the concrete parameterization. As a trade-off for broader applicability, the results are generally more conservative than those using the Orig. DER model.

In a comparison of both stability criteria, the Circle criterion is always superior to the Robust one. For the networks shown, this even applies to the comparison of [Robust, Orig. DER]

[5]If a deadband is assumed, the $Q(V)$-characteristic slope m is higher than the enclosing slope of the nonlinearity sector β, but limited through the maximum reactive power Q_{max} (cf. Fig. 3). This does not affect the applicability of the presented criterion but requires a downstream conversion from β to m.

[6]For PT_2-TAR approximation a worst case overshoot of $\xi = 15\ \%$ is set, instead the maximum closed loop gain for a broad range of parameterization is assumed as 1 for PT_2-DER and Orig. DER.

with [Circle, PT_2-TAR]. In addition, the simulative SA based on the CWT results in limits that are significantly higher than the Robust and Circle criteria for all benchmark networks. The trend of the results regarding the selected DER models and stability criteria is the same for all networks.

As an example, consider the results for the sDN1 network in Fig. 7. For the Circle criterion, using the DER model of type PT_2-TAR results in a stability limit of 19.1 $\%/\mathrm{pu}$ versus 30.8 $\%/\mathrm{pu}$ using PT_2-DER. With the Orig. DER model the stability can even be guaranteed up to a slope of 55.2 $\%/\mathrm{pu}$. This limit then still has a margin to the result of the simulative SA (Wavelet) at 77 $\%/\mathrm{pu}$. Furthermore, the discussed results are significantly less conservative than the 7.0 $\%/\mathrm{pu}$ for Orig. DER applying the Robust criterion. In addition, they are above the recommendation given in the network code [39], which is $m_{\max} = 20\ \%/\mathrm{pu}$.

We conclude, that with better knowledge of the DER model and it's parameterization, a higher slope can be considered acceptable. Furthermore, the results of the Robust criterion are always the most conservative, followed by the Circle criterion at a considerable distance. Except for sDN2, the results of the Circle criterion also exceed the recommended limit of the network code. Here, analytical approaches provide a reliable and fast SA. If the DSO needs to increase the $Q(V)$ slopes beyond the calculated limits of the Circle criterion or performing cross-validation, the presented simulative approach using the CWT allows for automated SA. The trade-off for less conservative results is the long simulation time. Furthermore, the secure application of a distributed $Q(V)$ fallback control for a centralized network-wide setpoint-based voltage control is conceivable as presented in [10].

VII. Conclusion

The authors present ongoing work on the evaluation of MIMO reactive power control systems in distribution networks. The work focuses on the interdependent $Q(V)$-characteristic voltage control. The presented approach can be used to support voltage management in distribution networks with high DER penetration by providing $Q(V)$-control to DERs across the grid. Subsequently, an analytical method for stability assessment based on the Circle Criterion was introduced. The new method enables the computation of a guaranteed stability limit for the $Q(V)$-characteristic slope taking into account the model parameters of the DER plant. The input variables required are the node admittance matrix $\underline{\boldsymbol{Y}}$, the network operating point $\mathcal{O}$, and the detailed DER model $G(s)$. As a substitute for a detailed DER model, a plant model approximation $G_{\mathrm{PT}_2}(s)$ based on a second order linear transfer function can be used. The stability assessment methods were applied to four different high-voltage benchmark networks. The results show a higher guaranteed stability limit compared to the previous work [27] as well as the German network code recommendations [39]. For verification, RMS simulations were performed in *PowerFactory* for each benchmark network. In addition, a wavelet transform based method was presented to automatically evaluate the RMS time series.

Future work will focus on fine-tuning of the Morse mother wavelet, additional assessment criteria, diverse network modeling and the dependence of the network operating point. It is planned to adopt other approaches, such as [49], [50], for the stability assessment of nonlinear systems. The presented criterion should be compared with the assessment approach of [21], [25], [51] in the time-discrete domain.

In contrast, a more direct approach is to use a static network model (cf. [52]) to opens up new possibilities for stability evaluation. However, to take advantage of this modeling approach, the voltage support must be implemented via an $I(U)$-characteristic instead of a $Q(V)$-characteristic.

References

[1] S. Krahmer, S. Ecklebe, P. Schegner, and K. Röbenack, "Analysis of the converter-driven stability of Q(V)-Characteristic control in distribution grids," in *Proc. IEEE 5th Int. Conf. Smart Energy Syst. Technol.*, 2022, pp. 1–6.

[2] M. Zhao, X. Yuan, J. Hu, and Y. Yan, "Voltage dynamics of current control time-scale in a VSC-Connected weak grid," *IEEE Trans. Power Syst.*, vol. 31, no. 4, pp. 2925–2937, Jul. 2016.

[3] M. Chiandone, R. Campaner, V. Arcidiacono, G. Sulligoi, and F. Milano, "Automatic voltage and reactive power regulator for wind farms participating to TSO voltage regulation," in *Proc. IEEE Eindhoven PowerTech*, 2015, pp. 1–5.

[4] O. Marggraf and B. Engel, "Experimental and field tests of autonomous voltage control in german distribution grids," in *Proc. IEEE PES Innov. Smart Grid Technol. Conf. Europe*, 2018, pp. 1–6.

[5] H. Zhu and H. J. Liu, "Fast local voltage control under limited reactive power: Optimality and stability analysis," *IEEE Trans. Power Syst.*, vol. 31, no. 5, pp. 3794–3803, Sep. 2016.

[6] G. Cavraro and R. Carli, "Local and distributed voltage control algorithms in distribution networks," *IEEE Trans. Power Syst.*, vol. 33, no. 2, pp. 1420–1430, Mar. 2018.

[7] A. Singhal, V. Ajjarapu, J. Fuller, and J. Hansen, "Real-time local volt/var control under external disturbances with high PV penetration," *IEEE Trans. Smart Grid*, vol. 10, no. 4, pp. 3849–3859, Jul. 2019.

[8] S. Asadollah, R. Zhu, and M. Liserre, "Analysis of voltage control strategies for wind farms," *IEEE Trans. Sustain. Energy*, vol. 11, no. 2, pp. 1002–1012, Apr. 2020.

[9] X. Zhou, M. Farivar, Z. Liu, L. Chen, and S. H. Low, "Reverse and forward engineering of local voltage control in distribution networks," *IEEE Trans. Autom. Control*, vol. 66, no. 3, pp. 1116–1128, Mar. 2021.

[10] F. Thomas, S. Krahmer, and P. Schegner, "Robust and optimized voltage droop control considering the voltage error," in *Proc. IEEE Power Energy Student Summit*, 2019, pp. 1–5.

[11] M. Kreutziger, P. Schegner, S. Wende-von Berg, M. Braun, and N. Bornhorst, "Reactive power management of distributed generators for selective voltage optimization in 110-kV-Subtransmission grids," in *Proc. IEEE Conf. Sustain. Energy Supply Energy Storage Syst.*, 2018, pp. 1–7.

[12] A. Inaolaji, A. Savasci, and S. Paudyal, "Distribution grid optimal power flow in unbalanced multiphase networks with Volt-VAr and volt-watt droop settings of smart inverters," *IEEE Trans. Ind. Appl.*, vol. 58, no. 5, pp. 5832–5843, Sep./Oct. 2022.

[13] N. Hatziargyriou et al., "Definition and classification of power system stability - revisited & extended," *IEEE Trans. Power Syst.*, vol. 36, no. 4, pp. 3271–3281, Jul. 2021.

[14] "Commission regulation (Eu) 2016/631 of 14 April 2016 establishing a network code on requirements for grid connection of generators (RFG)," *Official J. Eur. Union*, vol. L 112, pp. 1–68. [Online]. Available: https://op.europa.eu/en/publication-detail/-/publication/1267e3d1-0c3f-11e6-ba9a-01aa75ed71a1/language-en

[15] Y. Qian, X. Yuan, and M. Zhao, "Analysis of voltage control interactions and dynamic voltage stability in multiple wind farms," in *Proc. IEEE Power Energy Soc. Gen. Meeting*, 2016, pp. 1–5.

[16] B. Heimbach et al., "Contribution of a wind farm to voltage and system stability: Results of a measurement campaign," *CIRED Open Access Proc. J.*, vol. 2017, pp. 1646–1649, Oct. 2017.

[17] F. Andren, B. Bletterie, S. Kadam, P. Kotsampopoulos, and C. Bucher, "On the stability of local voltage control in distribution networks with a high penetration of inverter-based generation," *IEEE Trans. Ind. Electron.*, vol. 62, no. 4, pp. 2519–2529, Apr. 2015.

[18] M. Lindner and R. Witzmann, "On the stability of Q(V) in distribution grids," in *Proc. IEEE PES Innov. Smart Grid Technol. Conf. Europe*, 2018, pp. 1–6.

[19] F. Hans and W. Schumacher, "Modeling and small-signal stability analysis of decentralized energy sources implementing Q(U) reactive power control," in *Proc. IEEE 11th Int. Conf. Compat. Power Electron. Power Eng.*, 2017, pp. 588–593.
[20] J. H. Braslavsky, L. D. Collins, and J. K. Ward, "Voltage stability in a grid-connected inverter with automatic volt-watt and Volt-VAR functions," *IEEE Trans. Smart Grid*, vol. 10, no. 1, pp. 84–94, Jan. 2019.
[21] I. Murzakhanov, S. Gupta, S. Chatzivasileiadis, and V. Kekatos, "Optimal design of Volt/VAR control rules for inverter-interfaced distributed energy resources," *IEEE Trans. Smart Grid*, vol. 15, no. 1, pp. 312–323, Jan. 2024.
[22] M. Farivar, L. Chen, and S. Low, "Equilibrium and dynamics of local voltage control in distribution systems," in *Proc. IEEE Conf. Decis. Control*, 2013, pp. 4329–4334.
[23] P. Jahangiri and D. C. Aliprantis, "Distributed Volt/Var control by PV inverters," *IEEE Trans. Power Syst.*, vol. 28, no. 3, pp. 3429–3439, Aug. 2013.
[24] A. Eggli, S. Karagiannopoulos, S. Bolognani, and G. Hug, "Stability analysis and design of local control schemes in active distribution grids," *IEEE Trans. Power Syst.*, vol. 36, no. 3, pp. 1900–1909, May 2021.
[25] J. Schmitt, S. Ecklebe, and S. Krahmer, "An extended stability criterion for grids with Q(V)-controlled distributed energy resources," in *Proc. IEEE Power Energy Student Summit*, 2023, pp. 1–6.
[26] M. Hau and M. Shan, "Stability of fast Q(U) voltage droop control of wind parks in high voltage distribution grids," in *Proc. Conf. Sustain. Energy Supply Energy Storage Syst.*, 2017, pp. 1–6.
[27] S. Krahmer, A. Saciak, J. Winkler, P. Schegner, and K. Robenack, "On robust stability criteria for nonlinear voltage controllers in electrical supply networks," in *Proc. IEEE Power Syst. Computation Conf.*, 2018, pp. 1–7.
[28] F. Thomas, S. Krahmer, J. Winkler, P. Schegner, and K. Röbenack, "On grid modeling for stability assessment of droop voltage control," in *Proc. IEEE PES Innov. Smart Grid Technol. Conf. Europe*, 2019, pp. 1–5.
[29] W. Bounoua, M. F. Aftab, and C. W. P. Omlin, "Controller performance monitoring: A. survey of problems and a review of approaches from a data-driven perspective with a focus on oscillations detection and diagnosis," *Ind. Eng. Chem. Res.*, vol. 61, no. 49, pp. 17735–17765, 2022.
[30] M. Jelali and B. Huang, *Detection and Diagnosis of Stiction in Control Loops: State of the Art and Advanced Methods*. Berlin, Germany: Springer, 2010.
[31] E. Naghoosi and B. Huang, "Wavelet transform based methodology for detection and characterization of multiple oscillations in nonstationary variables," *Ind. Eng. Chem. Res.*, vol. 56, no. 8, pp. 2083–2093, 2017.
[32] E. A. Martinez-Ríos, R. Bustamante-Bello, S. Navarro-Tuch, and H. Perez-Meana, "Applications of the generalized morse wavelets: A review," *IEEE Access*, vol. 11, pp. 667–688, 2023.
[33] S. Krahmer, "Application of stability analysis of Q(V)-Characteristic controls related to the converter-driven stability in distribution networks. code ocean capsule," 2024 [Online]. Available: https://codeocean.com/capsule/4423034/tree/v1
[34] K. O. Papailiou, Ed. *Springer Handbook of Power Systems*. Berlin Germany: Springer, 2021.
[35] J. M. Garcia, "Voltage control in wind power plants with doubly FED generators," Ph.D. dissertation, Aalborg Univ., Aalborg, Denmark, 2010.
[36] J. Fortmann, *Modeling of Wind Turbines With Doubly Fed Generator System*. Berlin, Germany: Springer, 2015.
[37] *Wind Energy Generation Systems - Part 27-1: Electrical Simulation Models - Generic Models*, *IEC Standard 61400-27-1:2020*, International Electrotechnical Commission, Geneva, Switzerland, 2020.
[38] M. Lindner and R. Witzmann, "Modelling and validation of an inverter featuring local voltage control Q(V) for transient stability and interaction analyses," *Int. J. Elect. Power Energy Syst.*, vol. 101, pp. 280–288, 2018.
[39] VDE-AR-N 4120:2018-11, "Technical requirements for the connection and operation of customer installations to the high voltage network (TAR High Voltage)," VDE-AR-N 4120:2018-11, VDE, Berlin, Germany, Nov. 2018.
[40] H. K. Khalil, *Nonlinear Systems*, 3rd ed. Hoboken, NJ, USA: Prentice-Hall, 2002.
[41] R. Shorten, P. Curran, K. Wulff, C. King, and E. Zeheb, "On spectral conditions for positive realness of transfer function matrices," in *Proc. IEEE Amer. Control Conf.*, 2008, pp. 1076–1079.
[42] B. Boashash, *Time Frequency Signal Analysis and Processing: A Comprehensive Reference*. Amsterdam, the Netherlands: Elsevier, 2016.
[43] I. Kiskin, D. Zilli, Y. Li, M. Sinka, K. Willis, and S. Roberts, "Bioacoustic detection with wavelet-conditioned convolutional neural networks," *Neural Comput. Appl.*, vol. 32, pp. 915–927, 2020.
[44] O. A. Allan and W. G. Morsi, "A new passive islanding detection approach using wavelets and deep learning for grid-connected photovoltaic systems," *Elect. Power Syst. Res.*, vol. 199, 2021, Art. no. 107437.
[45] Y. Seyedi, J. Mahseredjian, and H. Karimi, "Impact of fault impedance and duration on transient response of hybrid AC/DC microgrid," *Elect. Power Syst. Res.*, vol. 197, 2021, Art. no. 107298.
[46] S. Meinecke et al., "SimBench-A benchmark dataset of electric power systems to compare innovative solutions based on power flow analysis," *Energies*, vol. 13, no. 12, 2020, Art. no. 3290.
[47] "Power System Data Model - A data model for the description of electrical power systems. GitHub repository," 2023. [Online]. Available: https://github.com/ieeh-tu-dresden/power-system-data-model
[48] "PowerFactory Tools - A toolbox for Python based control of DIgSILENT PowerFactory. GitHub repository," 2023. [Online]. Available: https://github.com/ieeh-tu-dresden/powerfactory-tools
[49] M. G. Safonov, "Stability of interconnected systems having slope-bounded nonlinearities," in *Proc. Anal. Optim. Syst.: 6th Int. Conf. Anal. Optim. Syst. Nice*, 2005, pp. 275–287. [Online]. Available: https://link.springer.com/chapter/10.1007/BFb0004960
[50] I. Lestas and G. Vinnicombe, "Scalable decentralized robust stability certificates for networks of interconnected heterogeneous dynamical systems," *IEEE Trans. Autom. Control*, vol. 51, no. 10, pp. 1613–1625, Oct. 2006.
[51] R. H. Gielen and M. Lazar, "On stability analysis methods for large-scale discrete-time systems," *Automatica*, vol. 55, pp. 66–72, 2015.
[52] S. Ecklebe, S. Krahmer, and K. Robenack, "A time-based approach to the modelling of power distribution grids," in *Proc. IEEE 25th Int. Conf. Syst. Theory Control Comput.*, 2021, pp. 425–430.

Sebastian Krahmer received the Dipl.-Ing. degree. He is currently a Research Associate with the Institute of Electrical Power Supply and High Voltage Engineering, TUD Dresden University of Technology, Dresden, Germany. Since 2019, he has been a Group Leader of the Planning and Operation of Grids Working Group. His research interests include the design of operation management concepts, the contribution of distributed generation plants to system services, and related stability assessment methods.

Stefan Ecklebe received the Dipl.-Ing. degree. He is currently a Research Associate with the Institute of Control Theory, TUD Dresden University of Technology, Dresden, Germany. His research interests include the modeling and control of systems with spatially distributed parameters in crystal growth applications and modeling and stability analysis of electrical networks with distributed generation plants.

Peter Schegner (Senior Member, IEEE) is currently the Director of the Institute for Electrical Power Supply and High Voltage Technology, TUD Dresden University of Technology, Dresden, Germany. He is in charge of numerous research projects in the fields of planning and operation of electrical networks, quality of supply, design and operation of smart grids, selective protection and automation technology, and stability of electrical network.

Klaus Röbenack is currently the Director of the Faculty of Electrical Engineering and Information Technology, Institute for Control Theory, TUD Dresden University of Technology, Dresden, Germany. His research interests include the design of nonlinear controllers and observers and scientific computing.